

Microscopy of Bioelectric Potentials using Electrochromism

Burhan Ahmed,¹ Erica Liu,^{2,3} Lothar Maisenbacher,¹ Pengwei Sun,^{4,3} Dana Griffith,¹ Kenneth Nakasone,¹ Yuecheng Zhou,^{5,6} Bianxiao Cui,^{2,3} and Holger Müller^{1,7,*}

¹*Department of Physics, University of California, Berkeley, California, USA*

²*Department of Chemistry, Stanford University, Stanford, California, USA*

³*Wu Tsai Neurosciences Institute, Stanford University, Stanford, California, USA*

⁴*Department of Radiology, Stanford University, Stanford, California, USA*

⁵*Department of Materials Science and Engineering, The Grainger College of Engineering, University of Illinois Urbana-Champaign, Urbana, Illinois, USA*

⁶*Department of Bioengineering, The Grainger College of Engineering, University of Illinois Urbana-Champaign, Urbana, Illinois, USA*

⁷*Molecular Biophysics and Integrated Bioimaging, Lawrence Berkeley National Laboratory, Berkeley, California, USA*

(Dated: January 30, 2026)

Studying the electrical signals generated by living cells is key to understanding numerous biological phenomena. Electrochromic optical recording (ECORE) uses the electrochromism exhibited by certain materials to noninvasively measure these signals in real time. In this work, we report on the development of ECORE based on a high-NA microscope objective. We demonstrate the recording of extracellular action potentials from cardiomyocytes with single-cell resolution and a high sensitivity of $3\text{ }\mu\text{V}$, which compares favorably to the previous record for any ECORE setup. Combining ECORE with microscopy simplifies the optical setup, allows for the simultaneous imaging of specimens, and makes ECORE accessible to a broader community of researchers, allowing for a better understanding of the biological processes that are integral to life.

I. INTRODUCTION

Detecting, recording, and monitoring bioelectric activities is essential for understanding a wide range of physiological functions such as memory formation [1, 2], muscle contraction [3], and the beating of the heart [4]. In cardiomyocytes, for example, monitoring changes in the action potential can help identify the safety and efficacy of drugs [5, 6]. Methods to detect these potentials have been studied for many decades, with significant improvements over time to the signal-to-noise ratio and spatial resolution, among other aspects [7, 8].

Electrode-based methods include the patch clamp [9, 10], which measures the large intracellular signal but is limited to short-term recording of very few recording sites due to its relatively large size and invasive nature. Measuring extracellular potentials by, e.g., multi-electrode arrays [11, 12], is less invasive and allows multichannel recording, but is limited to the fixed positions of the electrodes.

Optical recording allows flexibility to choose multiple areas of interest in a specimen. Well-established methods use genetically-encoded fluorescent indicators that respond to bioelectric activities such as calcium concentration and voltage changes [7, 13], but extended recording at a rapid rate is difficult due to photobleaching. Also, phototoxicity can compromise membrane integrity, while the introduction of the indicators can affect membrane capacitance [13]. Various label-free optical tech-

niques have been proposed in response to these limitations [14–19].

One such label-free method is electrochromic optical recording (ECORE), which is based on the electrochromism [20] in materials such as poly(3,4-ethylenedioxythiophene) polystyrene sulfonate (PEDOT:PSS, here referred to as PEDOT) [21, 22] and other dioxythiophene-based polymers [23]. In ECORE, cells are typically cultured on a PEDOT device (a glass slide coated with a thin film of PEDOT). Electrical potentials generated by the cells change the refractive index of the PEDOT film. Thus, by monitoring the power of a laser beam reflected off the device, these potentials can be measured. ECORE is noninvasive, allows recording from user-selected areas of interest, and is suitable for long-term recording: cells show no adverse reaction to PEDOT and can be measured over multiple recording sessions spanning many weeks [21–23]. ECORE recordings have a high sensitivity and have been shown to resolve electrical signals down to $3.3\text{ }\mu\text{V}$ [23], enabling the measurement of individual extracellular action potentials. Real-time recordings of action potentials associated with spontaneous activity from cardiomyocytes, neurons, and brain slices have already been demonstrated [21–23].

In published ECORE setups, light is focused using a simple lens and directed towards the sample through a prism [21–23]. This prism is coupled to the device slide using immersion oil; if the light is incident at the sample at supercritical angles, it is totally internally reflected and re-emerges from the other open face of the prism where it is sent to a detector. This geometry is challenging to align due to the oblique incidence angles and also requires separate imaging optics to observe the specimen.

* Contact author: hm@berkeley.edu

The incorporation of a microscope objective in ECORE is thus very desirable – a high-numerical aperture (high-NA) objective can, in principle, simplify the alignment (since it can both direct the incident light to the sample at supercritical angles and collect the reflected light). The same objective can also be used for imaging, allowing simultaneous observation of a sample and the recording of its bioelectric potentials. However, the small reflectance changes (parts per thousand or lower) that need to be detected make it necessary to minimize technical noise, which has so far prevented the use of microscopes in ECORE. Noise from the interference of multiple light reflections in the objective (parasitic reflections), and the increased sensitivity to environmental vibrations due to the higher magnification and complexity of the objective, are of particular concern.

Here we report on microscope ECORE, which utilizes a high-NA total internal reflection objective to record bioelectric potentials, and use it to record spontaneous action potentials from cultured human induced pluripotent stem cell (hiPSC)-derived cardiomyocytes. Using a light source that is less susceptible to interference, along with vibration damping, we are able to record with high signal-to-noise ratios (SNRs) and achieve a detection limit of $3\text{ }\mu\text{V}$, which slightly improves on the previous-best limit for any ECORE method. We use the same objective for imaging and show recordings of extracellular action potentials from different regions of one cardiomyocyte. By combining ECORE with microscopy, we have introduced a path to a broader implementation of ECORE for the label-free recording of bioelectric potentials.

II. EXPERIMENTAL SETUP

Microscope ECORE is shown in Fig. 1(a). To mitigate the effects of vibrations on our experiment, the setup breadboard is placed on a floating, damped optical table. We also ensure that all optical elements are mounted to the table rigidly to prevent residual environmental vibrations from perturbing the beam paths. The setup is placed in an enclosure with opaque panels to reduce the amount of environmental light reaching the detector.

We use 510-nm light as PEDOT shows a strong electrochromic response at this wavelength [22, 23]. The choice of light source is also important. High-NA objectives, such as the one we use, can contain more than 10 lens elements [24]. At the detector, small reflections from closely-spaced optical elements can interfere if the path length difference of the two interfering beams is less than the coherence length of the light. We use a superluminescent diode (SLD) (EXS210115-00, Exalos) since it has a short coherence length of $\sim 8\text{ }\mu\text{m}$. Therefore, parasitic reflections with a path length difference $>8\text{ }\mu\text{m}$ will not interfere with one another, strongly suppressing this source of technical noise.

The light from the SLD is split into two paths using a Wollaston polarizer which can also help prevent par-

asitic reflections as it separates the beams by oblique angles (20° in our case). One of these paths leads directly to one eye of a differential photodetector: this path serves as our reference beam. The remainder of the light (the signal beam) travels along the other path where it is first expanded using two plano-convex lenses to a $1/e^2$ intensity radius of $\sim 2\text{ mm}$ and is then directed towards the epi-illumination port of a commercial microscope (Eclipse Ti-U, Nikon). Here, an $f = 500\text{ mm}$ achromatic doublet lens is used to focus the light onto the back focal plane (BFP) of a 100x, 1.49-NA microscope objective (MRD01991, Nikon). The $f = 500\text{ mm}$ lens is also used to change the angle of incidence (AOI) at the sample plane of the objective by laterally moving the focused beam at the BFP of the objective. This simplifies the alignment as changing the AOI is simply a matter of translating the lens. The objective then focuses the beam onto the sample, as shown in Fig. 1(b). At the sample, any local changes in the electrical potential are converted into small changes in the index of refraction of the PEDOT film which result in small changes in the reflectance of the sample. Thus potential changes in the sample can be observed by monitoring the reflectance using a detector.

The reflected beam is collected by the objective and directed towards the other eye of the differential photodetector. This homemade photodetector (as described previously in [21–23]) is used to increase the sensitivity of detection by reducing any common-mode noise, such as intensity noise from the light source, by manually balancing the light power impinging on both eyes of the detector. To remove high-frequency noise (and prevent aliasing in the digitized signal), the detector output is filtered using a physical low-pass filter (with a cutoff frequency $\ll 5\text{ kHz}$) and then digitized with a sampling rate of 10 kHz and recorded.

We use glass coverslips ($22 \times 22 \times 0.15\text{ mm}^3$) coated with indium tin oxide (ITO) (CB-90IN, Delta Technologies) as the substrates for our PEDOT devices. We attach a custom 3D printed poly(lactic acid) sample well with a circular bottom opening of diameter 6 mm to the top of each substrate. PEDOT is then electrodeposited onto the substrate using the protocol described in [22], creating a thin film with an area of 28.3 mm^2 . The PEDOT film thickness depends on the duration of electrodeposition – a longer deposition time results in a thicker film.

The spatial resolution in ECORE is determined by the spot size of the beam at the sample [21]. Fig. 1(c) shows a section from an image of a typical cardiomyocyte sample recorded using a separate objective with a larger field of view. The $1/e^2$ spot sizes from various ECORE methods are also shown (superposed ellipses). When compared with the cardiomyocytes, the original ECORE beam [21] (large circle), and the dual-color ECORE beam [22] (central ellipse) are approximately the size of whole cells or large regions of whole cells. In contrast, the microscope ECORE beam (rightmost ellipse) is smaller by a factor of 2 compared to the the dual-color beam, the

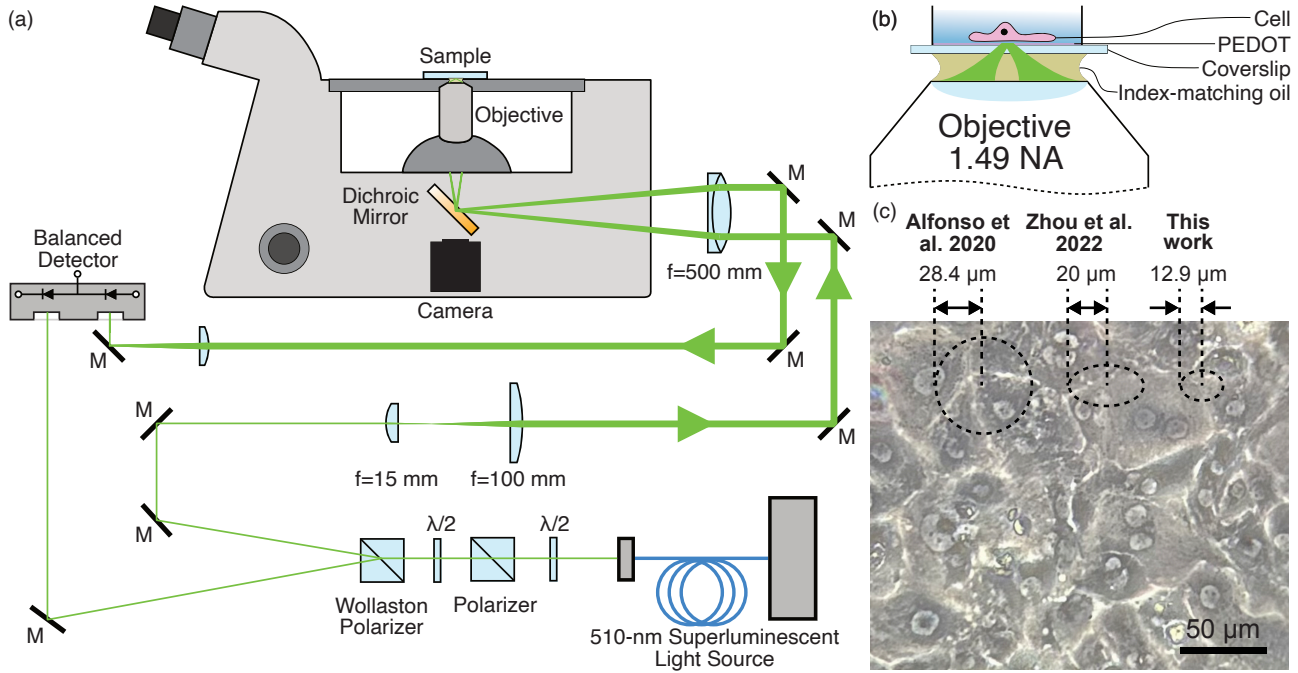


FIG. 1. (a) Schematic drawing of microscope ECORE. M: mirror, $\lambda/2$: half-wave plate. All components, except for the light source, are placed on an optical breadboard measuring 36×24 inches. (b) Detail showing the focused light at the sample. (c) A section of a microscope image (from a separate objective) showing a typical sample of cardiomyocytes. The dashed ellipses superposed on the image depict the $1/e^2$ intensity radius spot sizes of various ECORE beams. From left to right: original ECORE [21], dual-color ECORE [22], and microscope ECORE.

previously smallest ECORE beam. We are therefore able to probe the potential from smaller regions of these cardiomyocytes.

Because of the oblique incident angle, the microscope ECORE beam makes an elliptical spot on the specimen. The spot size, measured by fitting Gaussian functions to the intensity profiles of both axes of the spot, is $12.9 \times 9.4 \mu\text{m}^2$ (semi-major and semi-minor axis at $1/e^2$ intensity, respectively). With a typical light power of $600 \mu\text{W}$ entering the microscope base and an objective transmittance of $\sim 83\%$, approximately $500 \mu\text{W}$ of light reaches the sample. The light intensity impinging on the sample is therefore 131 W cm^{-2} . If desired, the spatial resolution can be further improved to $\sim 3.89 \mu\text{m}$ using the simple illumination scheme that we use, or to $\sim 138 \text{ nm}$ using annular illumination (see Appendix A). In practice, however, reducing the spot size increases the light intensity at the sample, causing perturbations to the cells. This can limit the recording duration as we discuss later.

III. RESULTS

A. Cell-Free Characterization of Microscope ECORE

To characterize our experimental apparatus, we use a potentiostat configured to apply a 1-mV, 1-Hz square

wave to a conducting ionic solution of $1 \times$ phosphate-buffered saline (PBS) in contact with the PEDOT film. We then measure the optical response by recording the output of the detector. This output is converted into a normalized change in the reflectance of the sample ($\Delta R/R$, where R is the reflectance of the sample) to provide a standardized metric for evaluating a PEDOT device. A higher $\Delta R/R$ value is preferable for a given applied voltage. A typical recording is shown in Fig. 2(a). This ECORE response, from a standard PEDOT film of area 28.3 mm^2 , has a 10% to 90% rise time of $\tau_r = (47 \pm 2) \text{ ms}$. As previously observed [21–23], $\tau_r \propto \sqrt{A_s}$, where A_s is the active sensing area of a PEDOT film. This can be modeled by a resistor-capacitor circuit as noted in [21]. For a large cardiomyocyte with an area of $2000 \mu\text{m}^2$, we expect $\tau_r = 0.4 \text{ ms}$. Therefore, the films provide optical responses that are fast enough to resolve bioelectric potentials from these cells.

We studied the effect that the thickness of the PEDOT film has on $\Delta R/R$. We prepared films of varying thicknesses by performing electrodeposition for 20 s, 40 s, 60 s, and 80 s. The average film thickness of these samples was measured using a profilometer (Dektak XT-S, Bruker) to be $(25 \pm 8) \text{ nm}$, $(51 \pm 6) \text{ nm}$, $(70 \pm 6) \text{ nm}$, and $(94 \pm 6) \text{ nm}$, respectively. We find that $\Delta R/R$ increases as the PEDOT film thickness is increased (black circles in Fig. 2(b)). However, we also find a sharper decrease in the reflectance of the samples as the film thickness increases (green triangles in Fig. 2(b)). Therefore, as

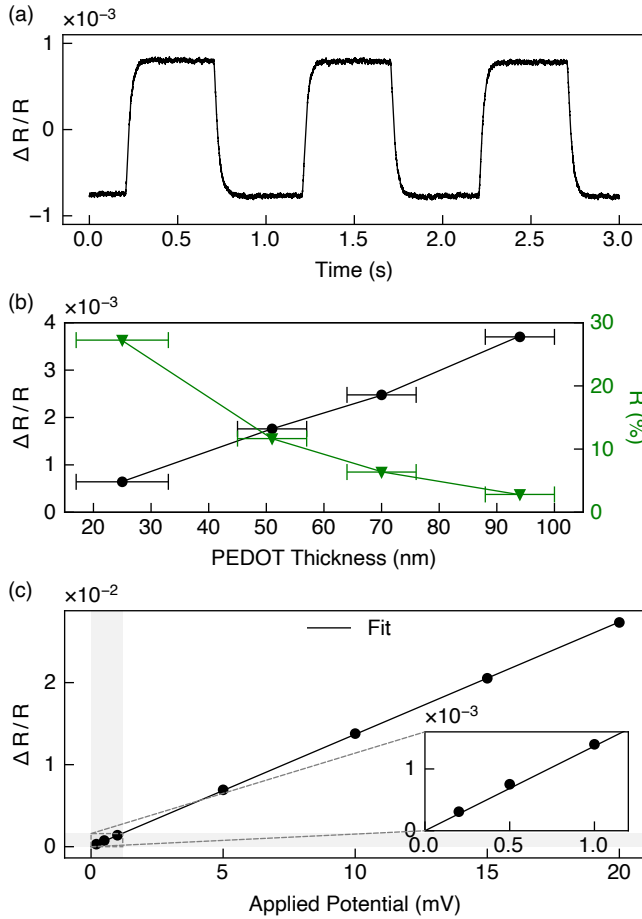


FIG. 2. (a) Detector output (in units of normalized change in the reflectance of the sample $\Delta R/R$) in response to a 1-mV, 1-Hz applied square wave at a bias voltage of 0 mV (with respect to a standard Ag/AgCl electrode). A 0.01-Hz high-pass digital filter (first-order Bessel) has been applied to flatten the baseline. (b) $\Delta R/R$ in response to a 1-mV, 1-Hz (at zero bias) applied square wave as a function of the PEDOT film thickness (black circles and line). The reflectance R of the samples is also shown (green triangles and line). (c) $\Delta R/R$ as a function of the amplitude of the applied square wave at zero bias. The line is a linear fit to the data described by the equation $y = (1.3696 \pm 0.0023) \times 10^{-3} x$. The inset shows data points near the origin.

the films gets thicker, less light reaches the detector and the SNR is reduced for the same input power. While in principle this loss of power can be compensated for by increasing the input power, in practice we cannot do so arbitrarily because high input powers can heat up the film, damaging biological cells. A good balance of high $\Delta R/R$ and R is found for films that are ~ 50 nm thick. We therefore perform all future experiments with films prepared for this thickness.

We also studied how $\Delta R/R$ changes as we vary the magnitude of the applied square wave at zero bias (Fig. 2(c)). A linear fit to the data gives a slope of $(1.3696 \pm 0.0023) \times 10^{-3} \text{ mV}^{-1}$ and accurately models the data

points. The optical response of PEDOT is thus linear with the magnitude of the applied voltage, in agreement with previous experiments. Therefore, changes in the potential are accurately represented by measuring $\Delta R/R$. Furthermore, if desired, a calibration curve such as the one shown in Fig. 2(c) can be used to convert the optically measured $\Delta R/R$ into extracellular voltage levels.

B. SNR and Detection Limit

Extracellular action potentials from cardiomyocytes have magnitudes of $\sim 100 \mu\text{V}$ [25, 26]. We confirmed that the noise level of our setup is low enough to detect such small signals by characterizing a 100-s-long microscope ECORE recording of a 1-mV, 1-Hz applied square wave at zero bias. The voltage spectral density of this recording is shown in Fig. 3(a). At lower frequencies, the noise level is higher than the shot noise limit (dashed red line) by about one order of magnitude, indicating there is still some room for improvement.

To evaluate the performance of our apparatus at this noise level, we also obtained the SNR for this recording. First, we digitally apply 0.01-Hz high-pass and 280-Hz low-pass filters to the data. We then compute the SNR for each cycle in the 100-s recording, as outlined in Fig. 3(b). The mean SNR for the entire recording of the 1-mV square wave is found to be 334 (dashed red line in Fig. 3(c)). The detection limit is defined as the potential that gives unity SNR. We thus estimate the detection limit of microscope ECORE to be $3 \mu\text{V}$. This result shows a successful reduction in technical noise to a level that is sufficient for detecting the typical cardiomyocyte extracellular potential. Despite the noise level being above the theoretical shot noise limit, we find that the SNR is still excellent and our detection limit is slightly better than the best limit that we have previously achieved with other iterations of ECORE.

C. Recording of Cardiomyocyte Action Potentials

We recorded the electrical activity from cultured human induced pluripotent stem cell (hiPSC)-derived cardiomyocytes using microscope ECORE (the cell culture protocol is described elsewhere [23]). One such recording is shown in Fig. 4(a). As expected from previous works [21–23], we find that the recording shows periodic signals associated with each beat. Zooming-in to any of the repeating features (4(a), right), we find a sharply peaked signal followed by a larger magnitude, longer-duration signal. We have previously confirmed that the sharp signal corresponds to the electrical signal from the cell, while the slower signal represents the mechanical contractions [21].

To focus on the electrical signals, which are of greater interest to us, we apply a 10 Hz high-pass filter to suppress the signals from the mechanical contractions. We

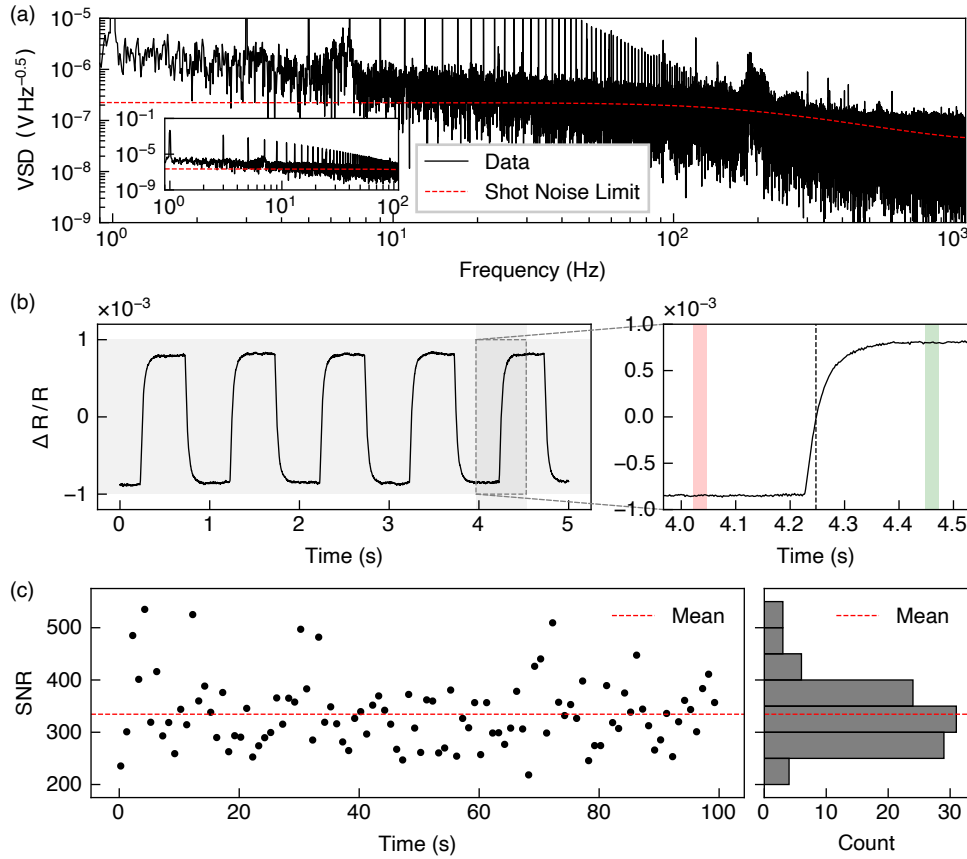


FIG. 3. (a) Voltage spectral density (VSD) of a 100-s-long microscope ECORE recording (black) in response to a 1-mV, 1-Hz square wave at zero bias. Peaks associated with the 1-Hz applied signal are visible and have been cropped to show the noise floor in more detail. The inset shows a zoomed-out version of the spectrum for lower frequencies. 600 μ W of light enters the microscope base and 44 μ W reaches the signal eye of the detector. The shot noise limit (see Appendix B) corresponding to the physical filter is also shown (dashed red line). (b) The left panel shows a 5-s section from the signal that was used to generate the VSD in (a) after the application of 0.01-Hz high-pass (first-order) and 280-Hz low-pass (third-order) digital Bessel filters. A zoomed-in section is shown in the right panel and illustrates the procedure for determining the SNR of one cycle from the entire 100-s recording. The dashed black line represents the time value associated with the half-amplitude of the cycle and is determined by first applying a Gaussian filter to smooth the data and then finding the peak of its derivative. The red and green shaded sections show 25-ms regions of the data 200 ms on either side of the dashed line. Linear fits are performed in both of these regions. The average standard deviation of the two fits determines the noise associated with the cycle, while the amplitude difference between the average $\Delta R/R$ in each region determines the signal for this cycle. (c) The SNR results from fitting all cycles in the 100-s recording (left). The mean SNR = 334 is also shown (dashed red line). A histogram of these SNR measurements is shown on the right.

also apply a 280 Hz low-pass filter to reduce noise from higher frequencies to improve the SNR (Fig. 4(b)). We can see that the electrical signal has clearly persisted through the application of the filters but the mechanical signal has been suppressed. These results demonstrate that we are able to record cardiomyocyte extracellular potentials with high SNRs.

We note that we can continuously record the action potentials from any region of a cardiomyocyte sample for at least 3 min. In some experiments, beyond this point, we observe damage to the cells which manifests itself as a reduction in the electrical and mechanical signal detected through ECORE as well as a visible reduction in the cell movement observed on the camera. We attribute

this relatively limited recording duration (compared to previous ECORE setups) to an increase in the light intensity at the sample owing to the smaller spot size of the beam. It is possible to obtain longer-term recordings by simply lowering the input power. While doing so reduces the SNR of the recording, we have obtained acceptable cardiomyocyte recordings for up to 7 min.

One significant benefit of microscope ECORE is that both the optical recording of the electrical potentials and the imaging of the specimen are done using the objective. This not only simplifies the imaging process, but also makes it easy to interact with the sample, the top of which is left completely accessible to the experimenter (Fig. 1(b)). We took advantage of this geometry to add

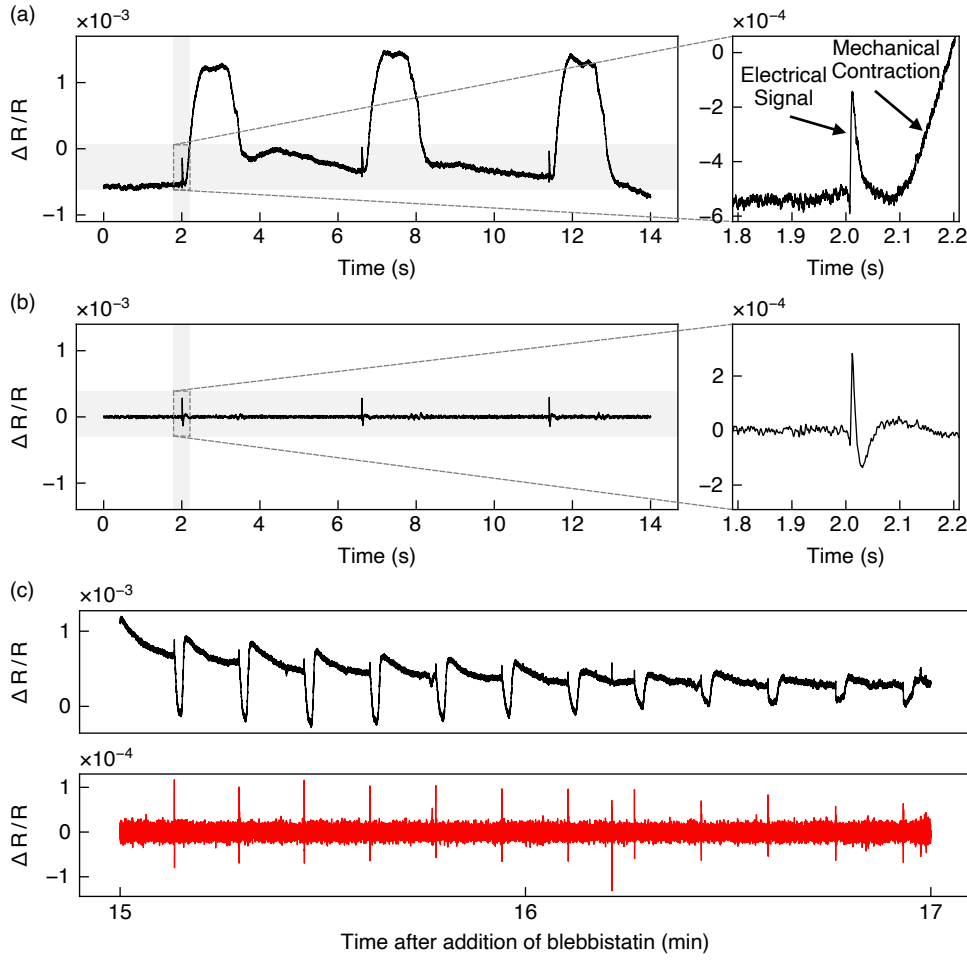


FIG. 4. (a) The ECORE signal from a cardiomyocyte is shown on the left. A zoomed-in section of the recording in shown on the right. The optical response from the electrical signal in the cells as well as the mechanical contraction are identified. (b) 10-Hz high-pass and 280-Hz low-pass filters (third-order Bessel) are applied to the data shown in (a). The right panel shows the effect of filtering: the electrical signal is still clearly visible but the mechanical contraction has been suppressed. (c) A 20 μ M solution of blebbistatin is added to a cardiomyocyte sample at $t = 0$ min. The black trace shows the recorded signal, where a 0.1-Hz high-pass first-order Bessel filter has been applied to flatten the recording baseline. The red trace shows the signal after the application of the 10-Hz high-pass and 280-Hz low-pass filters described in (b). The black trace shows that the mechanical signal is reduced over time, while the red filtered trace confirms that the electrical signal persists.

blebbistatin, a myosin inhibitor, to a cardiomyocyte sample in order to reduce mechanical contractions in the cells [21]. After the addition of blebbistatin at $t = 0$ min, we monitored the ECORE signal from the sample. To prevent optical damage to the cells, we only recorded for ~ 2 min from one cardiomyocyte before recording from another cell and repeating. A cell being studied at $t \approx 15$ min shows a clear decrease in the mechanical signal strength over time (black trace in Fig. 4(c)). When we filter out the mechanical signals altogether (red trace in Fig. 4(c)), we find that the electrical signals persist even as the mechanical signal is reduced. This observation re-confirms that the longer, larger spikes are mechanical in nature. Furthermore, this experiment demonstrates how the access provided to the sample could be used to study the effects of drugs on biological cells.

D. Recording Cardiomyocyte Action Potentials from Subcellular Regions

We next applied microscope ECORE to record the extracellular potentials from different regions of a single cardiomyocyte. In our experiments we keep the beam fixed in place and instead move the sample in any direction perpendicular to the optical axis of the objective using a translation stage. We can thus record the optical response from any user-designed region of interest by aligning the region with the known location of the beam. We did this for 9 regions of a cardiomyocyte, recording at each site (dashed ellipses in Fig. 5(a)) for 60 s. Sections of the resulting filtered ECORE recordings from each site are shown in Fig. 5(b). As the recordings were performed sequentially, we have manually aligned them in time to

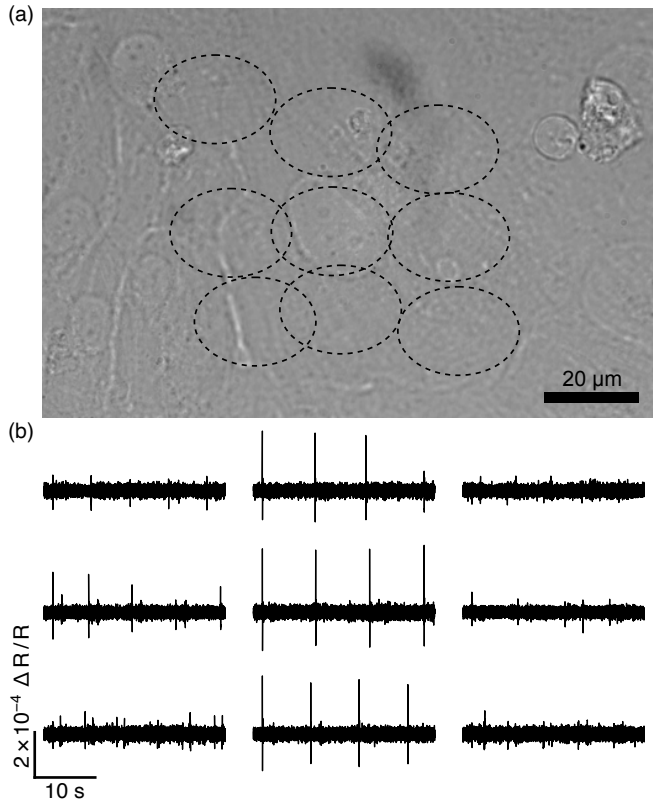


FIG. 5. (a) A cardiomyocyte (center) and its neighboring cells in the field of view of the 1.49-NA objective. The dashed ellipses show the location of the probing beam. The beam was moved to a particular spot, where the ECORE signal was recorded for 60 s before moving to another spot and repeating this process. (b) Sections of the recordings from the corresponding ellipses in (a) after the application of 10-Hz high-pass and 280-Hz low-pass filters (third-order Bessel). The recordings have been manually synchronized in time to facilitate comparison of the electrical signals in the different regions.

allow comparison of the electrical signals across the different regions. In this cell, the electrical activity appears to be stronger along the center of the cell and weaker elsewhere. This experiment demonstrates how microscope ECORE can be used to create a map of extracellular potentials from a given cell by recording from different regions in quick succession. It also illustrates the central role played by the objective, which enables the smaller spot size and allows for the simultaneous imaging and recording of a specimen.

IV. DISCUSSION

In this work, we report electrochromic optical recordings using a high-NA objective integrated into a commercial microscope. We demonstrate recordings with signal-to-noise ratios sufficient to reach a detection limit of $3 \mu\text{V}$, putting microscope ECORE on par with the most sensi-

tive ECORE method. We also demonstrate recordings of action potentials from cardiomyocytes and further utilize microscope ECORE to obtain a spatial map of the action potential from different regions of one cell.

The successful reduction of noise is crucial in allowing the combination of ECORE with microscopy. This integration provides several advantages compared to previous ECORE setups. As the objective can be used for both ECORE and imaging, it is possible to observe the sample in real time and choose cells to record electrical signals from without the need for separate optics for imaging. This setup, which is also simpler to align compared to previous iterations of ECORE, leaves the top of the sample completely accessible to the experimenter. This access can be used to easily exchange drug solutions with the sample (as we have shown) or to stimulate the sample with external electrodes, for example. We also highlight the relative simplicity of the construction that is needed to build the apparatus, which requires very few components altogether and has a compact footprint. Besides the high-NA microscope objective and the microscope base, all other optical elements in the setup (Fig. 1(a)) are inexpensive and easily obtained commercially.

The objective also allows an improvement in the spatial resolution of ECORE. However, one barrier to further improving the spatial resolution is the reduced recording duration due to the higher light intensities associated with smaller spot sizes. This limitation may be overcome in the future with the exploration of less absorptive electrochromic materials [23]. We also note that the recording of potentials from different sample regions is currently done sequentially (as opposed to simultaneously). In the future, we hope to combine a scanning technique (which we demonstrate in a separate manuscript under submission) with microscope ECORE to obtain simultaneous recordings from multiple points. For example, the signal beam could be scanned across different spots of the sample using an acousto-optic deflector (AOD). The AOD could be programmed to enable the recording of potentials from multiple user-designated spots simultaneously. This would allow researchers full control and spatial flexibility to study, in real time, the action potentials from a network of cells.

Microscope ECORE offers a simpler optical setup and alignment, improved spatial resolution, high recording sensitivity, and a further enhancement in the spatial flexibility over previous ECORE techniques. We therefore demonstrate microscope ECORE as a viable label-free recording method that can be utilized by researchers interested in studying bioelectric potentials, particularly those already using microscopy in their work. The introduction of ECORE into the world of microscopy not only allows for high-quality recording of extracellular action potentials, but also unlocks ECORE as an exciting tool that can be used to improve our understanding of the complex functioning of excitable cells.

ACKNOWLEDGMENTS

We would like to thank Ravichandra Venkateshappa and Professor Joseph Wu for providing the hiPSC-cardiomyocytes. We would also like to acknowledge Ashwin Singh and Professor Victoria Xu for their helpful discussions regarding microscope ECORE. Research reported in this article was supported by the National Institute of Neurological Disorder and Stroke of the National Institutes of Health under award number 1R01NS121934 (B.C. and H.M.). This work was also supported by a Stanford Bio-X Bowes Fellowship and the NIH Stanford Graduate Training Program in Biotechnology T32GM141819 (E.L.). Y.Z. acknowledges support from the American Heart Association Career Development Award (<https://doi.org/10.58275/AHA.25CDA1436867.pc.gr.229603>) and The Roy J. Carver Charitable Trust Individual Investigator Award. Part of this work was performed at nano@stanford RRID:SCR_026695.

Appendix A: Spatial Resolution

An important aspect of any microscopy technique is the spatial resolution. Here we consider the theoretical limits of the spatial resolution for microscope ECORE for two different illumination schemes.

1. Spot Illumination

We use the commonly defined resolution limit of an objective lens [27]:

$$r = \frac{1.22\lambda_0}{2\text{NA}},$$

where r is radius of the focused spot at the sample, λ_0 is the wavelength of the light, and NA is the numerical aperture of the lens. With complete illumination of the aperture, the diffraction-limited spot size of a 1.49-NA objective for light with $\lambda_0 = 510\text{ nm}$ would be $r = 209\text{ nm}$. However, for all incident light to undergo total internal reflection (TIR) as is desired in an ECORE setup, we can only illuminate a limited part of the aperture corresponding to supercritical incident angles.

The usable NA range is determined by the refractive indices of the four-layer structure containing the PEDOT thin film. Light enters the structure from index-matching oil ($n_0 = 1.518$) into a thin layer ($<30\text{ nm}$) of indium tin oxide ($n_1 \sim 1.84$) and a thin layer ($\sim 50\text{ nm}$) of PEDOT ($n_2 \sim 1.4$) before interacting with the last interface, i.e., water ($n_3 = 1.33$) [21]. For this system the critical angle is $\theta_c = \arcsin(n_3/n_0) = 61.2^\circ$ and the minimum NA that must be exceeded for TIR to occur is therefore $\text{NA}_{\min} = 1.33$ while the maximum NA is specified by the objective, in this case $\text{NA}_{\max} = 1.49$. Typical TIR illumination is

achieved by focusing light to a spot at the BFP of the objective using a lens (the $f = 500\text{ mm}$ lens in Fig. 1(a)). The smallest spot size at the sample that can be achieved with such illumination is therefore a focused spot at the BFP spanning the entire allowed NA range. Using the Abbe sine condition, we find that this maximal spot has $\text{NA} = 0.08$. Therefore, the smallest spot size that can be achieved with spot illumination is $r = 3.89\text{ }\mu\text{m}$. This is considerably larger than the spot size achieved through full illumination of the aperture. If desired, we could minimize our spot size at the sample to this value by ensuring maximal illumination of the allowed range of NA values at the BFP of the objective.

2. Annular Illumination

Another approach to achieving TIR at the sample is to illuminate the entire ring (annulus) of the BFP defined by the minimum and maximum NA values for supercritical illumination. The radial intensity profile of the diffraction pattern formed at the sample plane for this illumination scheme is given by [27]:

$$I \propto \frac{1}{r'^2} \left[J_1 \left(\frac{2\pi\text{NA}_{\max}r'}{\lambda_0} \right) - \beta J_1 \left(\frac{2\pi\text{NA}_{\min}r'}{\lambda_0} \right) \right]^2,$$

where r' represents the radial coordinate at the sample plane, J_1 is the Bessel function of the first kind of order 1, and $\beta \equiv \text{NA}_{\min}/\text{NA}_{\max}$. The first minimum of this profile occurs at $r' = 138\text{ nm}$, which is smaller than the first minimum location for the full aperture illumination (for which $r' = 209\text{ nm}$ as noted previously). However, as noted in [27], more of the intensity is spread into the higher orders of the diffraction pattern. Nevertheless, annular illumination represents one way in which the spatial resolution could be further improved if desired.

Appendix B: Shot Noise Limit

The current spectral density of shot noise associated with a current I is given by [28]:

$$S_I(f) = \sqrt{2eI},$$

where e is the elementary charge. The current generated by a photodiode is $I = P\mathcal{R}$, where \mathcal{R} is the responsivity of the photodiode. The photodiodes we use (FDS100, Thorlabs) have $\mathcal{R} = 0.177\text{ A W}^{-1}$ for 510-nm light. For a photodetector with a feedback resistance of R ($R = 100\text{ k}\Omega$ in our experiment), the voltage spectral density associated with shot noise is therefore:

$$S_V(f) = \sqrt{2eP\mathcal{R}R}.$$

Upon passing through a filter with a transfer function $G(f)$, this becomes:

$$S_{V,G}(f) = \sqrt{2eP\mathcal{R}R|G(f)|}.$$

The rms voltage associated with the shot noise can be computed by integrating the power spectral density (square of the voltage spectral density above) to obtain:

$$V_{\text{rms}}^2 = \int_0^{\infty} [S_{V,G}(f)]^2 df = 2eP\mathcal{R}R^2B,$$

where $B = \int_0^{\infty} |G(f)|^2 df$ is the filter noise bandwidth.

In the passband of a filter we have $|G(f)| = 1$ and the

voltage spectral density becomes:

$$\text{VSD}_{\text{shot}} = \sqrt{2eP\mathcal{R}R}.$$

Finally, this value must be multiplied by $\sqrt{2}$ to account for the fact that a differential photodetector outputs the difference of two photodiode currents. Therefore, with $P = 44 \mu\text{W}$, we have $\text{VSD}_{\text{shot}} = 2.24 \times 10^{-7} \text{ V Hz}^{-0.5}$.

[1] P. Liu and E. W. Miller, Electrophysiology, Unplugged: Imaging Membrane Potential with Fluorescent Indicators, *Acc. Chem. Res.* **53**, 11 (2020).

[2] N. Axmacher, F. Mormann, G. Fernández, C. E. Elger, and J. Fell, Memory formation by neuronal synchronization, *Brain Res. Rev.* **52**, 170 (2006).

[3] J. C. Calderón, P. Bolaños, and C. Caputo, The excitation-contraction coupling mechanism in skeletal muscle, *Biophys. Rev.* **6**, 133 (2014).

[4] G. M. Wahler, 52 - cardiac action potentials, in *Cell Physiology Source Book (Third Edition)*, edited by N. Spere-lakis (Academic Press, San Diego, 2001) third edition ed., pp. 887–898.

[5] S. Peng, A. E. Lacerda, G. E. Kirsch, A. M. Brown, and A. Bruening-Wright, The action potential and comparative pharmacology of stem cell-derived human cardiomyocytes, *J. Pharmacol. Toxicol. Methods* **61**, 277 (2010).

[6] O. Caspi, I. Itzhaki, I. Kehat, A. Gepstein, G. Arbel, I. Huber, J. Satin, and L. Gepstein, In Vitro Electrophysiological Drug Testing Using Human Embryonic Stem Cell Derived Cardiomyocytes, *Stem Cells Dev.* **18**, 161 (2009).

[7] M. Scanziani and M. Häusser, Electrophysiology in the age of light, *Nature* **461**, 930 (2009).

[8] D. S. Peterka, H. Takahashi, and R. Yuste, Imaging Voltage in Neurons, *Neuron* **69**, 9 (2011).

[9] B. Sakmann and E. Neher, Patch Clamp Techniques for Studying Ionic Channels in Excitable Membranes, *Annu. Rev. Physiol.* **46**, 455 (1984).

[10] C. L. Hill and G. J. Stephens, An introduction to patch clamp recording, in *Patch Clamp Electrophysiology: Methods and Protocols*, edited by M. Dallas and D. Bell (Springer US, New York, NY, 2021) pp. 1–19.

[11] J. Pine, Recording action potentials from cultured neurons with extracellular microcircuit electrodes, *J. Neurosci. Methods* **2**, 19 (1980).

[12] R. Burley and J. R. M. Harvey, Multielectrode arrays, in *Patch Clamp Electrophysiology: Methods and Protocols*, edited by M. Dallas and D. Bell (Springer US, New York, NY, 2021) pp. 109–132.

[13] R. U. Kulkarni and E. W. Miller, Voltage Imaging: Pitfalls and Potential, *Biochemistry* **56**, 5171 (2017).

[14] Y. Zhou, E. Liu, H. Müller, and B. Cui, Optical electrophysiology: Toward the goal of label-free voltage imaging, *J. Am. Chem. Soc.* **143**, 10482 (2021).

[15] P.-C. Zhang, A. M. Keleshian, and F. Sachs, Voltage-induced membrane movement, *Nature* **413**, 428 (2001).

[16] S. Ae Kim, K. Min Byun, J. Lee, J. Hoon Kim, D.-G. Albert Kim, H. Baac, M. L. Shuler, and S. June Kim, Optical measurement of neural activity using surface plasmon resonance, *Opt. Lett.* **33**, 914 (2008).

[17] J. F. Barry, M. J. Turner, J. M. Schloss, D. R. Glenn, Y. Song, M. D. Lukin, H. Park, and R. L. Walsworth, Optical magnetic detection of single-neuron action potentials using quantum defects in diamond, *Proc. Natl. Acad. Sci. U.S.A.* **113**, 14133 (2016).

[18] H. J. Lee, D. Zhang, Y. Jiang, X. Wu, P.-Y. Shih, C.-S. Liao, B. Bungart, X.-M. Xu, R. Drenan, E. Bartlett, and J.-X. Cheng, Label-Free Vibrational Spectroscopic Imaging of Neuronal Membrane Potential, *J. Phys. Chem. Lett.* **8**, 1932 (2017).

[19] T. Ling, K. C. Boyle, V. Zuckerman, T. Flores, C. Ramakrishnan, K. Deisseroth, and D. Palanker, High-speed interferometric imaging reveals dynamics of neuronal deformation during the action potential, *Proc. Natl. Acad. Sci. U.S.A.* **117**, 10278 (2020).

[20] R. J. Mortimer, Electrochromic materials, *Annu. Rev. Mater. Res.* **41**, 241 (2011).

[21] F. S. Alfonso, Y. Zhou, E. Liu, A. F. McGuire, Y. Yang, H. Kantarci, D. Li, E. Copenhaver, J. B. Zuchero, H. Müller, and B. Cui, Label-free optical detection of bioelectric potentials using electrochromic thin films, *Proc. Natl. Acad. Sci. U.S.A.* **117**, 17260 (2020).

[22] Y. Zhou, E. Liu, Y. Yang, F. S. Alfonso, B. Ahmed, K. Nakasone, C. Forró, H. Müller, and B. Cui, Dual-Color Optical Recording of Bioelectric Potentials by Polymer Electrochromism, *J. Am. Chem. Soc.* **144**, 23505 (2022).

[23] Y. Zhou, E. Liu, A. M. Österholm, A. L. Jones, P. Sun, Y. Yang, C.-T. Tsai, T. Zaluska, W. Zhang, H. Müller, J. R. Reynolds, and B. Cui, Ultrasensitive label-free optical recording of bioelectric potentials using dioxythiophene-based electrochromic polymers, *Nat. Commun.* **16**, 6776 (2025).

[24] D. B. Murphy and M. W. Davidson, Lenses and geometrical optics, in *Fundamentals of Light Microscopy and Electronic Imaging* (John Wiley & Sons, Inc., Hoboken, NJ, USA, 2012) pp. 53–77.

[25] N. Klauke, G. L. Smith, and J. Cooper, Extracellular Recordings of Field Potentials from Single Cardiomyocytes, *Biophys. J.* **91**, 2543 (2006).

[26] T. Kaneko, H. Toriumi, J. Shimada, and F. Nomura, Extracellular field potential recording of single cardiomyocytes in agarose microchambers using microelectrode array, *Jpn. J. Appl. Phys.* **57**, 03EB03 (2018).

[27] D. Axelrod, Optical configurations and setup, in *Total Internal Reflection Fluorescence (TIRF) and Evanescent Microscopies*, 2053–2563 (IOP Publishing, 2022) pp. 5–1 to 5–32.

[28] P. Horowitz and W. Hill, Low-noise techniques, in *The Art of Electronics* (Cambridge University Press, 2015)

pp. 473–593.